Available online at www.sciencedirect.com
ScienceDirect
Geochimica et Cosmochimica Acta 71 (2007) 2190–2208
Geochimica et Cosmochimica Acta
www.elsevier.com/locate/gca

The effects of soil type and chemical treatment on nickel speciation in refinery enriched soils: A multi-technique investigation

David H. McNear Jr. [a,*], Rufus L. Chaney [b], Donald L. Sparks [c]

[a] *Rhizosphere Science Research Group, Department of Plant and Soil Sciences, N122S Agricultural Sciences North Building, University of Kentucky, 1100 Nicholasville Road, Lexington, KY 40546-0091, USA*
[b] *USDA-ARS, Animal Manure and Byproducts Laboratory, Beltsville, MD 20705, USA*
[c] *Environmental Soil Chemistry Research Group, Department of Plant and Soil Sciences, 152 Townsend Hall, University of Delaware, Newark, DE 19717-1303, USA*

Received 25 July 2006; accepted in revised form 6 February 2007; available online 20 February 2007

Abstract

Aerial deposition of Ni from a refinery in Port Colborne, Ontario, Canada has resulted in the enrichment of 29 km^2 of land with Ni concentrations exceeding the Canadian Ministry of the Environment's remedial action level of 200 mg kg^{-1}. Several studies on these soils have shown that making the soils calcareous was effective at reducing chemically extractable Ni, as well as alleviating Ni phytotoxicity symptoms in vegetable crops grown in the vicinity of the refinery. Conversely, dolomitic limestone additions resulted in increased uptake of Ni in the Ni hyperaccumulator *Alyssum murale* 'Kotodesh', a plant whose use was proposed as a remediation strategy for this area. In this paper we use multiple techniques to directly assess the role soil type and lime treatments play in altering the speciation of Ni in the Welland loam and Quarry muck soils around the refinery and relate these findings to Ni mobility and bioavailability.

Stirred-flow dissolution experiments using pH 4 HNO_3 showed that Ni release from the limed Quarry muck and Welland loam soils was reduced (~0.10%) relative to the unlimed soils (~2.0%). Electron microprobe analysis (EMPA) identified approximately spherical NiO and Ni metal particles, which are associated with no other metals, and range from 5 to 50 μm in diameter. Synchrotron micro-X-ray absorption fine structure and X-ray fluorescence spectroscopies showed that Ni and Al layered double hydroxide (Ni–Al LDH) phases were present in both the limed and unlimed mineral soils, with a tendency towards more stable (e.g., *aged*-LDH and phyllosilicate) Ni species in the limed soil, possibly aided by the solubilization of Si with increasing pH. In the muck soils, Ni–organic complexes (namely fulvic acid) dominated the speciation in both limed and unlimed soils.

The results reported herein show that both soil type and treatment have a pronounced effect on the speciation of Ni in the soils surrounding the Port Colborne refinery. We provide the first evidence that Ni–Al LDH phases can form in anthropogenically enriched mineral field soils at circumneutral pH, and can lead to a reduction in Ni mobility. In the organic soils Ni is strongly complexed by soil organic matter; a property enhanced with liming. Interestingly, increased accumulation of Ni by *A. murale* grown in the limed muck and loam soils indicates that the plant may be capable of removing Ni from those fractions typically considered unavailable to most plants.

* Corresponding author. Fax: +1 859 257 3655.
E-mail address: dave.mcnear@uky.edu (D.H. McNear Jr.).

0016-7037/$ - see front matter © 2007 Elsevier Ltd. All rights reserved.
doi:10.1016/j.gca.2007.02.006

1. INTRODUCTION

Nickel (Ni) comprises roughly 0.016% of the Earth's crust, making it the 24th most abundant metal (Burkin, 1987). Once regarded as a waste product in the copper smelting process (known as "devils copper" or "kupfernickel" from which it bears its name), Ni now has many uses with the most prominent being as a component (in concert with Cr, Nb, Mo, Ti) in stainless steel (Bacon et al., 2002). Acquisition of Ni involves beneficiation of the metal from both laterite (i.e., oxide) and sulphide ores, with most coming from the latter because of the lower energy requirements necessary for extraction. Removing and concentrating metals has primarily relied on pyrometallurgical processes in which the impurities in the ore are "cooked off" leaving behind an enriched matte (Nriagu, 1996). During this process acid forming compounds (e.g., SO_2, Cl, etc.) as well as particulates of varying composition and morphology are produced and, prior to adequate emission standards, released into the environment (Hoflich et al., 2000). As a result, vast areas of soil enrichment and, in some cases, the complete perturbation of the ecosystem surrounding metal processing facilities have occurred.

The operation of a nickel refinery in Port Colborne, Ontario, Canada from 1918 to 1984 has resulted, through aerial deposition, in the enrichment of roughly 345 km^2 of soils with greater than 45 mg/kg Ni. As reported by several researchers (Temple and Bisessar, 1981; Frank et al., 1982; Bisessar, 1989), farms in the immediate vicinity of the refinery have soil Ni concentrations ranging from 600- to 10,000-mg/kg which resulted in a reduction in vegetable crop yields (the primary activity on the muck soils surrounding the facility). As such, the Canadian Ministry of the Environment (MOE) established a phytotoxicity based guideline of 200 mg/kg above which remediation is deemed necessary (Kuja et al., 2000). An estimated 29 km^2 surrounding the facility are above the established remediation guideline. The large area of enriched soils makes remediation by conventional methods (i.e., excavation and disposal) impractical because of the associated high costs (>US$3 million/hectare) (Raskin et al., 1997). As an alternative, in situ stabilization, in which amendments are added to the soil in an effort to promote long-term sequestration of the metal/s, may be more practical, especially if the objective is to simply alleviate Ni phytotoxicity.

Several researchers have examined how in situ stabilization has influenced the Ni mobility and bioavailability in the mineral and muck soils found around the Port Colborne refinery. Bisessar (1989) found that increasing the soil pH with $Ca(OH)_2$ was effective at reducing the phytoavailable Ni fraction (i.e., ammonium acetate extractable) and thus eliminating Ni toxicity in celery grown in the Ni enriched muck soils. Kukier and Chaney (2001) found a similar reduction in phytoavailable ($SrNO_3$ and DTPA extractable) Ni for oat, wheat and red beet grown in both the mineral and muck soils amended with dolomitic limestone. Similarly, Kukier and Chaney (2004) found that soil liming was effective at alleviating Ni toxicity in 11 agronomically important crops grown in the mineral soils. As a long-term solution, they proposed making the soils calcareous (i.e., addition of excess lime) to buffer the acidifying potential of agronomic fertilizers and acid rain.

A promising alternative or supplement to in situ methods is the use of specialized metal accumulating plants (hyperaccumulators) which are able to remove and concentrate metals in their shoots. The Kotodesh cultivar of the Ni hyperaccumulating plant *Alyssum murale* has been evaluated for use in phytomining of Ni from the soils surrounding the Port Colborne refinery. In phytomining, the plants are harvested, the dry-matter incinerated for energy and the remaining ash refined to recover the entrained metals (Li et al., 2003). While investigating the effect of pH on nickel phytoextraction efficiency, they found a counterintuitive response of increased Ni uptake with increased pH. In most cases, increasing soil pH results in less plant available metal (as the previous studies with vegetable crops showed). The pH response of *A. murale* may provide a unique opportunity to combine in situ stabilization methods (i.e., limestone additions) with phytomining.

For phytoremediation to be effective, it is necessary for the plant to extract enough metal to make recovery economical, and more importantly, to avoid diluting the metal into several more tons of metal enriched plant biomass than the original amount of contaminated soil. With both in situ stabilization and phytoremediation, the speciation of the metal in the soils is of utmost importance, as it determines how effective the additive is at sequestering the metal, and dictates how bioavailable the metal is for uptake by plants.

The use of synchrotron radiation techniques has revolutionized the way we investigate metal speciation in environmental systems. Using synchrotron X-rays, the speciation of metal in a sample can be directly assessed, because it requires no sample treatment. The first synchrotron methods relied on bulk X-ray absorption fine structure spectroscopy (XAFS), which used a relatively large beam size (i.e., mm^2). Because natural samples are heterogeneous, bulk-XAFS methods are only capable of determining the average speciation within the mm^2 of sample analyzed. However, with the development of better optics, we are now able to focus the X-ray beam down to square microns (μm^2) and thus probe within heterogeneous systems. With this ability, special care must be taken to assure that the data collected are representative of the speciation in the whole system. Several statistical approaches have been used to limit the potential subjectivity imposed by this type of analysis. Among them, principle component analysis and linear least squares fitting have been the most successful. Manceau et al. (2002) have outlined a procedure for using synchrotron-based techniques to properly ascertain metal speciation within soil samples. By using bulk XAFS, it is possible to find the compositionally dominant species within the sample, and then using micro-spectroscopic tools such as μ-XAFS, μ-SXRF (synchrotron X-ray fluorescence) and μ-XRD (X-ray diffraction) minor yet potentially more reactive components can be detected. There are an increasing number of examples in the literature where this approach has been used (Sarret et al., 2002; Nachtegaal et al., 2005; Voegelin et al., 2005).

To evaluate the effectiveness of soil treatments on Ni mobility and plant availability in Port Colborne soils, the previous studies (Frank et al., 1982; Kukier and Chaney, 2000; Kukier and Chaney, 2001; Kukier and Chaney, 2004) used chemical extractants (i.e., $Sr(NO)_3$, DTPA, ammonium acetate). None, however, has used direct methods to assess the change in chemical speciation of Ni within the soils affected by remediation or soil type. As such, the objectives of this study are to investigate the influence of past in situ remediation efforts (liming) and soil type (organic vs. mineral) on the speciation of Ni and evaluate how the speciation has impacted Ni mobility and bioavailability.

2. MATERIALS AND METHODS

2.1. Soil collection, characterization and sample preparation

Soils were collected in November 2002 from field plots maintained by the United States Department of Agriculture (USDA) on land located adjacent to a historic Ni refinery near the town of Port Colborne, Ontario, Canada. The research plots were established in 1999 to explore the ameliorative effects of liming on Ni toxicity to selected crop plants as well as the phytoextraction potential of the Ni hyperaccumulator *Alyssum murale*. In 1999, selected sites received a dolomitic lime treatment of 88 dry metric tons/ha, followed by another treatment of 33 Mt/ha in the spring of 2000. Soils are of the Welland (Typic Epiquoll; Canadian classification, Orthic Humic Gleysol) and Quarry muck (Terric Haplohemist; Canadian classification, Terric Mesisol) series. Sites were selected based on soil type (organic or mineral) and treatment (limed or unlimed) from which several representative sub-samples were collected from the plow-layer (upper 20 cm) of each plot and then homogenized in 20 gal Rubbermaid™ tubs. Soils were sieved moist past a 2 mm sieve and then stored for future analysis.

The fraction of sand, silt and clay was determined using the Bouyoucos Hydrometer method. Pretreatment of the soil to remove soluble salts and carbonates, organic matter, and metal oxides followed by wet settling and centrifugation was conducted to isolate the <2 μm fraction for mineralogical analysis via X-ray diffraction (Lavkulic and Wiens, 1970). The pH of the air-dried soils was determined using a soil to deionized water ratio of 1:2 (w/v) with a 1 h equilibration time. Soil organic matter content was determined using the loss-on-ignition (LOI) method. The cation exchange capacity (CEC) of each soil was determined using the Compulsive Exchange Method (Sumner and Miller, 1996). Free iron and aluminum oxide content of the soils was determined using the sodium-citrate-bicarbonate-dithionite method (Mehra and Jackson, 1960). Total metal contents of the soil samples were determined using a microwave assisted acid (HNO_3 and HCl) digestion (US Environmental Protection Agency 1995 Method 3051). The soils were analyzed for total Ni, Cd, Co, Cu, Fe, Pb, and Zn content via Inductively Coupled Plasma Atomic Emission Spectrometry (ICP-AES). For XAFS analysis, subsamples of the <2 mm fraction from the limed and unlimed, mineral and muck soils, that were not pretreated, were embedded in Scotchlight® (3 M) electrical resin after which they were sectioned to 30 μm and mounted on pure quartz slides.

2.2. Stirred-flow dissolution studies

A stirred-flow reactor similar to that described by Strawn and Sparks (2000) was employed to study the dissolution of Ni from limed and unlimed Welland loam and Quarry muck soils as well as α-$Ni(OH)_2$, *fresh* Ni–Al LDH, NiS and NiO reference materials. Nitric acid (HNO_3, pH 4) was used as a dissolution agent to mimic natural weathering processes as would occur via acid rain, fertilizer additions or root exudates in the rhizosphere.

The stirred-flow reactor consists of a 7.5 ml chamber which is positioned on top of a stir plate where effective mixing (400 rpm) is provided via a stir bar in the reaction chamber. Approximately 0.3 g of each soil and 3 mg of the reference was added to the reaction chamber. The amount of reference material used was determined by calculating the average amount of Ni in each soil (i.e., 300 mg of soil containing ~1% Ni = 3 mg Ni). The flow of desorbing solution, supplied at a constant flow by a peristaltic pump, enters the bottom side of the chamber, is mixed thoroughly, and then exits through the top. To prevent loss of the material within the reaction chamber, a 25 mm diameter, 0.22 μm filter is inserted at the top prior to the outlet. The solution leaving the reaction chamber is then sent to a fraction collector where the samples are deposited in 18 ml HDPE test tubes. The desorbing solution flow rate was no greater than 0.8 ml/min (48 ml/h) in order to ensure a proper residence time within the mixing chamber and to minimize re-adsorption of Ni onto the soil. Samples were collected every 5 min for the first hour and every 10 min thereafter for a total of 8 h. Based on preliminary studies, 8 h was sufficient time for the reaction to reach an apparent steady-state in Ni dissolution. Twelve, 4 ml samples were generated in the first hour followed by 42, 8 ml samples for the remaining 7 h, resulting in a total of 54 samples per dissolution experiment. Supernatants were analyzed for Ni content using ICP-AES. Data are presented as chamber volumes (CV) versus the concentration (mg/l) of Ni being released from the reaction chamber. Chamber volumes were calculated by multiplying the flow rate by the time and dividing by the volume of the chamber.

2.3. Electron microprobe analysis (EMPA)

Subsamples of the limed and unlimed mineral and muck soils were prepared for EMPA analysis by first embedding them in Scotchlight® electrical resin after which they were thin sectioned to 30 μm and mounted on pure quartz slides. Prior to analysis the thin sections were sputter coated with carbon and then examined on a JEOL JXA-8600 microprobe (John Hopkins University) with wavelength and energy dispersive detectors (WDS and EDS, respectively). Samples were first scanned manually from 50 to 300× using back-scattered electron (BSE) imaging to find regions of high nickel concentration after which EDS and WDS were used to generate elemental maps for Ni, O, Ca, Al, K, Mg, Fe, Cu and Si.

2.4. Bulk XAFS standard preparation, data collection and characterization

A total of 33 Ni standards were generated, purchased, or compiled from previous work published by the UD environmental soil chemistry group, and were used to identify the unknown species present in the soils. Bunsenite (*green*-NiO), millerite (NiS), arupite ($Ni_3(PO_4)_2$) and $NiCO_3$ were obtained from Johnson Matthey. The minerals trevorite ($(Ni,Cu)Fe_2^{3+}O_4$), heazlewoodite (Ni_3S_2), godlevskite ($(Ni_{8.7},Fe_{0.3})_9S_8$) and gaspeite ($(Ni,Mg,Fe)CO_3$) were obtained from Excaliber (Peekskill, NJ). Mineral samples were prepared by grinding to a fine powder in a ceramic ball-mill or mortar and pestle. The coprecipitate α-$Ni(OH)_2$ was prepared following the methods of Génin et al. (1991). The β-$Ni(OH)_2$ was generated by aging the initial α-$Ni(OH)_2$ precipitate under a nitrogen atmosphere at 298 K for 1 month. Freshly precipitated (i.e., no aging) Ni–Al LDH (NO_3 in the interlayer) was taken from Scheinost et al. (1999) where they prepared the sample as described in Taylor (1984). The aged Ni–Al LDH was acquired from Peltier et al. (2006) and was generated by incubating an initial Ni–Al LDH (CO_3 in the interlayer) precipitate (prepared as in Taylor (1984)) for 2 weeks at 65 °C. The same Ni–($Al(OH)_3 + SiO_2$), Ni–SiO_2, Ni–gibbsite, Ni–talc and Ni–pyrophyllite generated by Scheckel and Sparks (2000) were used here except they had been aged a total of ~6 yrs (compared to the 2 yrs of aging in the aforementioned citation) in a 0.1 M $NaNO_3$ solution at constant temperature (298 K). The Ni–phyllosilicate spectrum was taken from Scheinost and Sparks (2000). The Ni–humic acid standard was taken from Nachtegaal and Sparks (2003), and was generated by dissolving 5 wt% HA in 0.05 M NaOH, precipitating the sample at pH 3 and then raising the pH to 7.5 and adding 3 mM Ni (as $NiNO_3$). The sample was then centrifuged and the solid collected and stored in the refrigerator as a wet paste until XAFS analysis. The Ni–Fulvic acid (Elliott soil fulvic acid 2S102F) standard was taken from Strathmann and Myneni (2004) and was analyzed as an aqueous solution. Aqueous organic standards were prepared as follows: Ni-aqueous, 30 mM $NiSO_4$; Ni–aconitate, 50 mM $NiSO_4$ + 150 mM aconitate; Ni–malate, 30 mM $NiSO_4$ + 300 mM malate; Ni–malonate, 30 mM $NiSO_4$ + 300 mM malonate; Ni–citrate, 30 mM $NiSO_4$ + 120 mM citrate; Ni–oxalate, 30 mM $NiSO_4$ + 300 mM oxalate; Ni–tartrate, 50 mM $NiSO_4$ + 500 mM tartrate; Ni–histidine, 30 mM $NiSO_4$ + 300 mM histidine; Ni–glutathione, 30 mM $NiSO_4$ + 300 mM glutathione; Ni–cystine, 30 $NiSO_4$ + 300 mM cystine; Ni–glycine, 30 mM $NiSO_4$ + 300 mM glycine. Samples were adjusted to pH 6.5 using HNO_3. ACS trace metal grade chemicals, acid washed containers and ultra-pure double-deionized (18.2 Ω Millipore) water were used to generate all standards.

XAS data for standards were collected on beamline X-11A at the National Synchrotron Light Source (NSLS), Brookhaven National Laboratory, Upton, NY (unless otherwise stated). The electron beam energy was 2.5–2.8 GeV with a maximum beam current of 300 mA. The monochromator consisted of two parallel Si (1 1 1) crystals with a vertical entrance slit opening of ~0.5 mm. The beam size on the sample was maintained at 2 × 10 mm for all samples and standards. Prior to data collection, the energy was calibrated to the first inflection point on the K adsorption edge of a Ni metal foil standard ($E_0 = 8.333$ keV for Ni). Solid samples were loaded into individual acrylic sample holders and sealed with Kapton™ tape. For aqueous standards, non-adhesive Kapton™ film was used to seal the sample chamber to avoid any interaction of the sample with the tape adhesive. The samples were then mounted 45° to the incident beam and data collected at the Ni K-edge over the energy range 8183–9082 eV in fluorescence mode using a N_2/Ar (95/5%) filled Lytle Cell. To optimize the Ni signal and remove elastically scattered radiation, the fluorescence signal was filtered using a Co foil, one to two sheets of Al foil and Soller slits. Harmonic rejection was achieved by detuning the monochromator 20% of I_o. Multiple scans ($\geqslant 3$) were collected for each sample to improve the signal-to-noise ratio.

XAS data analyses were performed using WinXAS 3.1 (Ressler, 1997). Prior to averaging, the individual spectra were background corrected and normalized. Background subtraction was performed by fitting a linear polynomial to the pre-edge region between 150 and 50 eV below the Ni K-edge. The edge jump was normalized to unity by fitting a linear polynomial between 100 and 500 eV above the Ni K-edge. The threshold energy (E_o) was determined by selecting the root of the second derivative through the absorption edge of the differentiated spectra, and used to convert the spectra from energy to k-space (photoelectron wave vector ($Å^{-1}$)). A cubic spline function with $\leqslant 7$ kn was then used to remove the contribution to the spectrum resulting from atomic absorption in the absence of backscattering contributions. This step generated the XAFS function ($\chi(k)$), which was then weighted by k^3, to compensate for dampening of the XAFS amplitude with increasing k, and then Fourier transformed. A Bessel window with a smoothing parameter of 3 $Å^{-1}$ was used in this step to reduce artifacts due to the finite Fourier filtering range of $\Delta k = 2$–10 $Å^{-1}$.

The first two major shells below 3.5 Å were individually selected ($R = \sim 1$–3.5), back-transformed and fit using a non-linear least squares fitting (NLLSF) approach and theoretical scattering paths generated using ATOMS and FEFF 7.02 software packages (Zabinsky et al., 1995). The Ni–Al LDH standards were fit with an R range below 6.4 Å ($R = \sim 1$–6.4)to include the weak backscattering contribution from Al occurring around 6.09 Å (Scheinost and Sparks, 2000). Ab initio phase and amplitude functions for Ni–O, Ni–Fe, Ni–Mn, and Ni–Al were generated from the refinement of hydrotalcite where Ni, Fe, or Mn were substituted for Mg in the octahedral layer, and from the structures of Trevorite ($[(Ni,Cu)Fe_2^{3+}O_4]$), Heazlewoodite (Ni_3S_2), Godlevskite ($(Ni_{8.7},Fe_{0.3})_9S_8$), and Gaspeite ($(Ni,Mg,Fe)CO_3$). The Ni–O and Ni–C (organic acids) phase and amplitude functions were generated using either nickel acetate tetrahydrate ($(Ni(CH_3COO)_2H_2O$) (Nicolai et al., 1998) or disaguabis(salicyladehydato) nickel ($Ni(sal)_2(H_2O)_2$) (Stewart et al., 1961) and Ni–N (amino acids) paths using Ni–Imidazole $(C_3H_4N_2)_6Ni(NO_3)_2$ (Santoro

et al., 1969). The parameters obtained fitting the individual shells were then refined using a multi-shell fit over the entire spectra in k space ($\Delta k = 2.1$–10.8). The energy shift parameters (E_0) were set equal for all paths and the root mean square disorders [RMSD (σ^2(Å^2))] or the Debye–Waller factor] and bond distance (R) were set equal for those metals sharing atomic shells. The amplitude reduction factor (S_0^2) was fixed at 0.85. The number of variables used in the fit were always much less then the number of independent points (NIP) calculated as $N_{pts} = 2\Delta k \Delta R/\pi$. Errors in the bond distance (R) are estimated to be $R \pm 0.02$ Å and $R \pm 0.05$ Å, and errors for the coordination number (CN) are estimated to be CN ± 20% and CN ± 40%, for the first (Ni–O/S/N) and second shells (Ni–Ni/Al/Si/C), respectively based on the fitting statistics and comparisons with previously published XRD and EXAFS data on similar systems (Scheidegger et al., 1998; O'Day et al., 1994).

2.5. μ-SXRF and μ-XAS data collection and analysis

μ-EXAFS and μ-synchrotron based X-ray fluorescence (μ-SXRF) data were collected on beamline 10.3.2 (1.9 GeV and 300 mA) at the Advanced Light Source, Lawrence Berkeley National Lab (Berkeley, CA) (Marcus et al., 2004). The soil thin sections were mounted to the sample stage aligned 45° to the incident beam. Fluorescence signals were collected using a Ge solid-state multi-element detector. To assess the spatial distribution of Ni and other elements in the samples, fluorescence maps were collected over 1000 μm^2 (coarse map) and 200 μm^2 (fine map) with a beam size of 16×7 μm and 5×5 μm and using a step size of 20 and 5 μm (in both x and y), respectively and an integration time of 100 ms. For mapping, the beam energy was set to 11 keV to allow for the detection of relevant elements including Ni, Fe, Co, Cu, Zn, and Mn. Using the map, data cross correlations were performed to determine element associations (e.g., Ni/Fe, Ni/Mn) within samples. The metal associations were evaluated using the Pearson's correlation coefficient(r) between the two element intensities on a per-pixel basis (Manceau et al., 2002). To determine the Ni speciation at points of interest (POI) in the maps, μ-XAS spectra were collected up to 500 eV above the Ni K-edge. The number of μ-XAS spectra collected at each point depended on the concentration at the POI (i.e., number of fluorescent counts). To obtain sufficient data quality (i.e., signal-to-noise) a minimum of 1 million total integrated fluorescence counts were collected, which resulted in a minimum of 3 scans per POI. Prior to μ-XAS data collection, the beamline energy was calibrated to the first inflection point of the Ni metal foil standard ($E_0 = 8.333$ keV).

Analysis of XAFS spectra collected from multicomponent systems (such as soils) is difficult with traditional fitting procedures in which atomic shells are individually selected and fit because the multiple metals in the system may have overlapping atomic shells making it difficult if not impossible to separate them. Therefore, to determine the species present within a mixed system, a dataset of spectra from multiple POI's throughout a sample are analyzed statistically using principal component analysis (PCA) (Wasserman et al., 1999). The PCA technique determines if the data set can be described as weighted sums of a smaller number of components, which would be the case if each point in the dataset is comprised of a smaller number of distinct compounds. Selection of the number of principal components was made where the empirical indicator (IND) and Eigenvalues were at their minimum (Malinowski, 1977). Target transformation (TT) is then used to identify the components by taking a spectrum of a known reference compound and mathematically removing from the spectrum anything that does not look like the principle components identified by PCA. If minimal information has to be removed from the known reference spectrum, then one can conclude it is most likely present in the sample. Reference spectra are evaluated for their "goodness of fit" by the SPOIL value (Malinowski, 1978). Generally, values <1.5 are considered excellent, 1.5–3 good, 3–4.5 fair, 4.5-6 poor and >6 unacceptable. After the contributing standard phases are identified, linear least squares fitting (LLSF) is used to determine the amount (%) of each standard within the individual sample spectra making up the dataset. The fit is optimized where the normalized sum squared ($NSS = \sum[k^3\chi(k)_{exp} - k^3\chi(k)_{reconstr.}]^2/\sum[k^3\chi(k)_{exp}]^2$) value is at a minimum. A reference phase was included in the fit only if it decreased the NSS by 20% or more. The accuracy of this fitting approach is dependent upon the data quality, the completeness of the standards data set, and the range over which the data were fit (Manceau et al., 2002).

3. RESULTS AND DISCUSSION

3.1. Soil characteristics

The physiochemical and mineralogical properties of the limed and unlimed Welland loam and Quarry muck soils are shown in Table 1. The organic matter (OM) content of the Quarry Muck field soil is ten times that of the Welland loam. However, the Welland soil possesses a substantial amount of OM compared to most soils, which is typical for soils formed in colder climates such as these Lake Plane soils.

The Ni, Co, Cu, and Zn concentrations in all of the soils are elevated, compared to normal background concentrations, resulting from refinery and other fallout from surrounding industries. The limed Welland and Quarry muck soils are 0.4 and 0.7 pH units above their unlimed counterparts, respectively.

3.2. Stirred flow dissolution studies

To evaluate the relative solubility of important Ni species present in these soils, stirred-flow experiments were performed on reagent grade NiS, green-NiO, α-Ni(OH)$_2$ and Ni–Al LDH reference compounds (Fig. 1). The obvious characteristic that this data reveals is the resistance of NiO followed by NiS to dissolution by HNO_3 at pH 4. At the completion of the 8-h dissolution experiment, 100% and 79% of the NiO and NiS remain, respectively. In contrast, the α-Ni(OH)$_2$ and (fresh) Ni–Al LDH

Table 1
Physiochemical and mineralogical properties of the limed and unlimed Welland Loam and Quarry Muck Soils

Soil	OM (%)	Particle size sand/ silt/clay (%)	CEC (meq/100 g)	pH	Ni (mg/kg)	Co (mg/kg)	Cu (mg/kg)	Fe (mg/kg)	Pb (mg/kg)	Zn (mg/kg)	Mineralogy of <2 μm clay fraction
Quarry muck											
Unlimed	71.7	51/34/15	49.2	5.8	4902	38.4	293	15,908	51.9	118	Kaolinite > Montmorillonite>
Limed	72.3		64.5	6.5	3516	59.9	426	20,049	63.9	164	Mica > Geothite > Quartz
Welland loam											
Unlimed	9.8	29/35/36	18.1	7.1	4700	50.1	475	13,860	64.8	181	Kaolinite > Mica > Geothite>
Limed	8.2		22.7	7.5	3468	31.5	300	13,198	37.1	101	Quartz

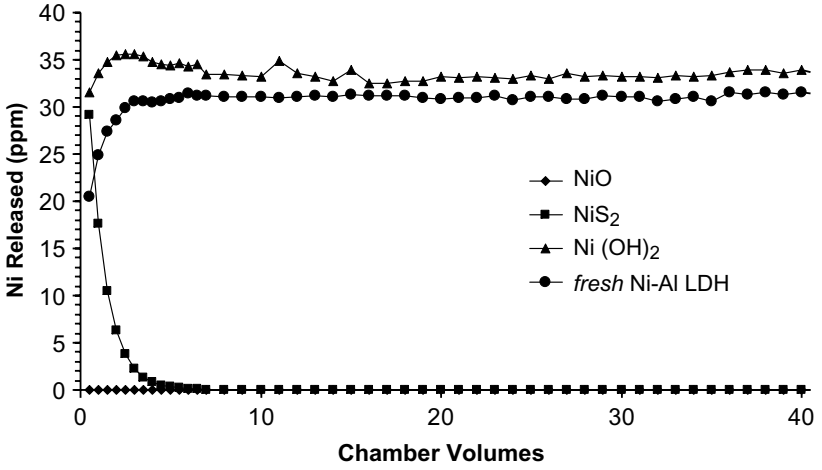

Fig. 1. Ni release from NiS_2, $Ni(OH)_2$, fresh Ni–Al LDH and NiO standards during an 8-h stirred-flow dissolution experiment using pH 4 HNO_3.

reference phases were characterized by an initially rapid release of Ni followed by a constant release with 57% and 62% of the total α-$Ni(OH)_2$and *fresh* Ni–Al LDH phases, respectively remaining after the 8-hr experiment. The results for α-$Ni(OH)_2$ and Ni–Al LDH are similar to those of Scheckel et al. (2000) in that the α-$Ni(OH)_2$ appears to be more soluble than the LDH phase.

The results for the stirred-flow experiments using the soils and pH 4 HNO_3as a dissolution agent are shown in Fig. 2. The influence of lime additions on the amount of

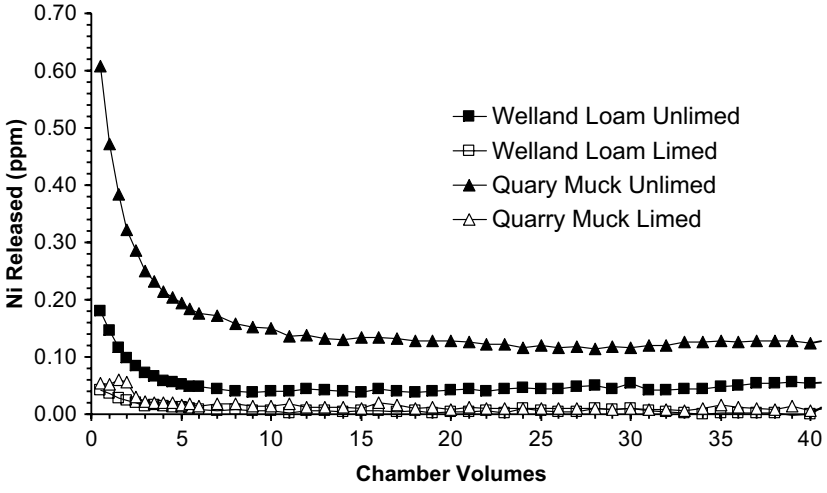

Fig. 2. Ni release from Welland loam and Quarry muck limed and unlimed soils during an 8-h stirred-flow dissolution experiment using pH 4 HNO_3.

Ni released from each of the soils is evident. Of the total nickel present in the Welland loam, ~2.0% was removed from the unlimed soil compared to 0.11% from the limed soil during the duration of the 8 h experiment. A similar trend was observed for the Quarry muck soils with ~2.3% and 0.10% Ni removal from the unlimed and limed muck soils, respectively. The reduction in Ni loss as a result of raising the pH indicates that liming may have altered the soil Ni speciation. These results corroborate findings by Kukier and Chaney (2004) who saw a similar reduction in $Sr(NO_3)_2$ extractable Ni with increasing pH.

3.3. Electron probe micro-analysis (EMPA)

Electron probe microanalysis was used to assess Ni associations with lower Z elements such as Al or Si which are undetectable via other methods employed in this study (e.g., XAFS). The backscattered electron images (black and white image) and associated elemental distributions (colored) for the Welland loam and Quarry muck, un-limed and limed soils can be seen in Figs. 3a,b and 4a,b, respectively. The most resounding feature among all of the soils and treatments is the presence of distinct approximately spherical Ni rich particles ranging from ~5- to 50 μm in diameter. Hoflich et al. (2000) and Weinbruch et al. (2002) examined Ni refinery aerosols and found similar spherical morphologies with variable chemical composition differentiated chiefly by the silica and sulfur contents. In our samples, the particles are not associated with any of the elements analyzed with the exception of oxygen. This is evident in the Welland loam unlimed sample (Fig. 3b). A particle has been dissected in the microtoming process, revealing the particle interior. The interior has darker spots in the center and a darker shell which correlates well with the O elemental map. The particle is most likely metallic Ni which has begun to weather, forming an oxide coating on its exterior.

Diffuse Ni associations are also visible in the elemental maps of both the limed Welland loam (Fig. 3a) and un-limed Quarry muck (Fig. 4b) soils (see arrows). In the bottom left corner of the Welland loam sample, Fe, Ni and Cu are well correlated on the surface of a K, Al and Si containing particle (possibly feldspar or mica). Nickel is well correlated with Cu throughout both the limed and un-limed muck samples. The most obvious example of the Ni–Cu association is shown in the top left corner of the Ni and Cu elemental maps of Fig. 4b where Ni and Cu are associated with a Si and O containing (most likely quartz) particle. Since these soils are extremely high in organic matter and Cu has a very high affinity for OM (followed by Ni), it is likely the Ni and Cu are complexed in an organic coating on the surface of the quartz particle.

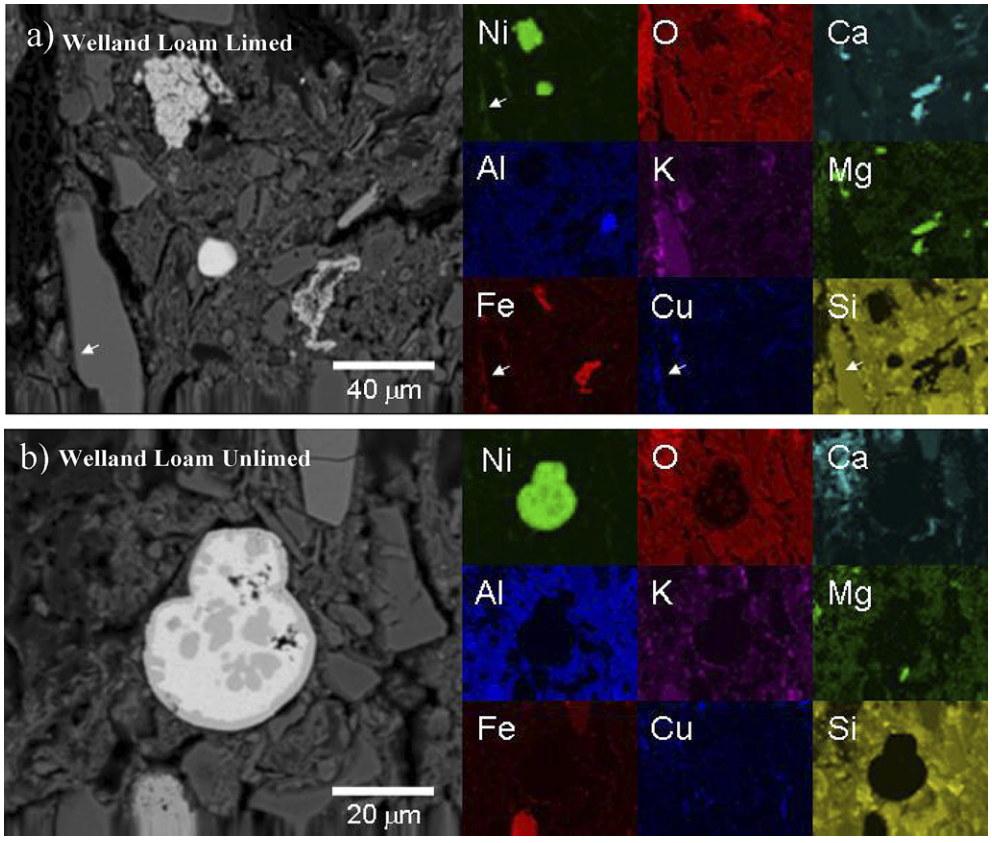

Fig. 3. Backscattered electron image (large) and elemental distribution maps (small) for the (a) limed and (b) unlimed Welland loam soils.

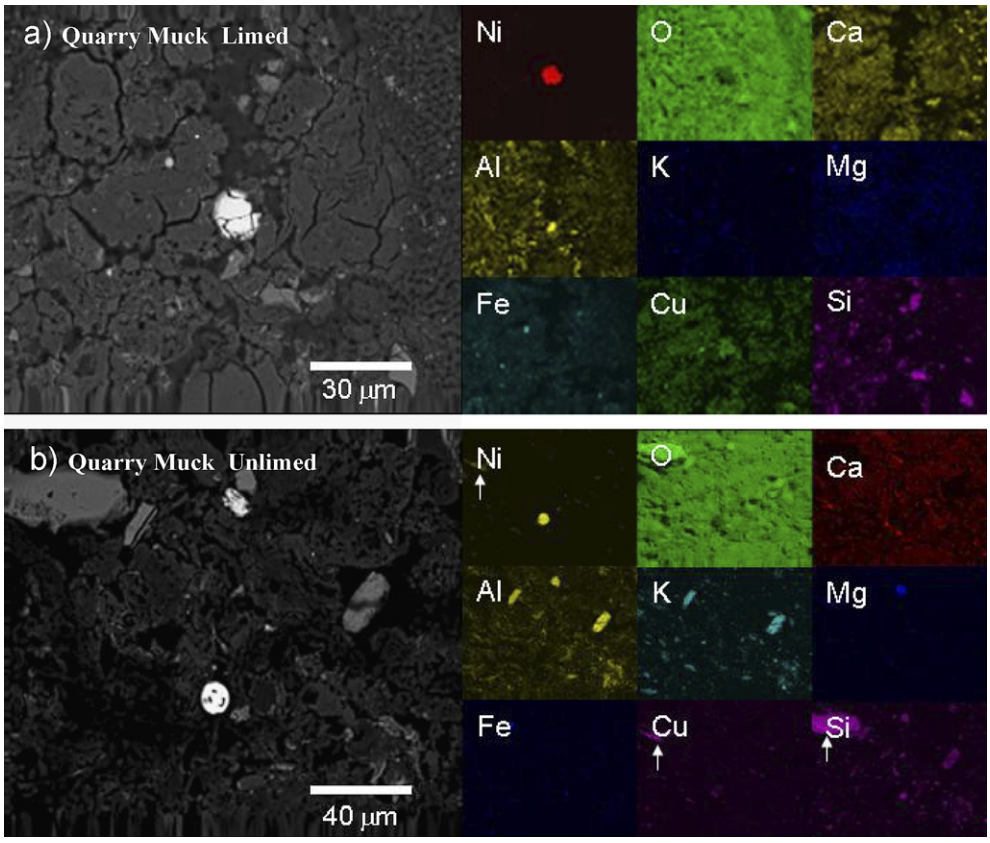

Fig. 4. Backscattered electron image (large) and elemental distribution maps for the (a) limed and (b) unlimed Quarry muck soils.

3.4. XAFS characterization of standards

When using principal component and target transform analysis, it is critical to have a well characterized set of reference phases representing all of the possible metal species present within the system under investigation. Fig. 5a and b shows the extracted $k^3\chi(k)$-spectra for some of the reference phases and Table 2, the structural parameters derived from NLLSF. The mineral standards used include bunsenite (NiO), trevorite ($(Ni,Cu)Fe_2O_4$), heazlewoodite (Ni_3S_2), godlevskite ($(Ni,Cu)_9S_8$), Millerite (NiS) and Gaspeite ($(Ni,Mg,Fe)CO_3$) which were identified by Weinbruch et al. (2002) (using transmission and scanning electron microscopy) as components in aerosols from a refinery processing nickel sulfide ores. The coordination number and bond distances for Bunsenite compare well with those reported in the literature (Trivedi et al., 2001). Nickel is in tetrahedral coordination in the sulfur bearing minerals with average Ni–S first shell distances of 2.3 Å. The NLLSF for Millerite were best achieved using 4.5 S atoms at approximately 2.3 Å, which represents the average bond distance for the S atoms (@2.264(2), 2.369(2) and 2.263(1) Å) in the rhombohedral structure (Grice and Ferguson, 1974). The NLLSF for the Heazlewoodite standard verifies its trigonal structure observed by Fleet (1977) with edge and point sharing tetrahedra containing Ni coordinated to 4 sulfur atoms at an average distance of 2.25 Å. The NLLSF for Godlevskite verifies its orthorhombic structure, with edge and point sharing tetrahedra and pyramids containing Ni surrounded by 4 or 5 S atoms at an average distance of 2.19–2.32 Å and a second coordination shell of ~4 Ni atoms at 2.52 Å.

A variety of sorption and coprecipitate standards were generated or obtained to represent all of the likely Ni sorption complexes expected within the soils The aged (6 year) Ni–$Al(OH)_3 + SiO_2$, Ni–talc and Ni pyrophyllite samples were best fit with ~4–6 Ni atoms at ~3.08 Å and ~5–8 Si atoms at ~3.25 Å in the second coordination shell, similar to that of Ni–phyllosilicate (Scheidegger et al., 1998; Scheinost et al., 1999; Scheckel and Sparks, 2000; Scheinost and Sparks, 2000; Nachtegaal and Sparks, 2003). These findings support the long term transformation from initial Ni–Al LDH or α-$Ni(OH)_2$ precipitates to Ni–Al phyllosilicate or Ni phyllosilicates predicted in Scheckel and Sparks (2001), with the exception of Ni–pyrophyllite, where best fits could only be obtained using Si and Ni in the second shell. However, with additional information obtained from polarized XAFS, diffuse reflectance spectroscopy (DRS), or with an extended data range and a more robust spectral analysis procedure (e.g., wavelet analysis) we may be able to distinguish whether a phyllosilicate or LDH phase has formed in these samples (work currently in progress). Regardless, these findings do support the formation of a more stable mineral precursor (i.e., Ni phyllosilicate and/or Ni–Al phyllosilicate) which is adequate as a standard for identifying the nature of the precipitates formed in the

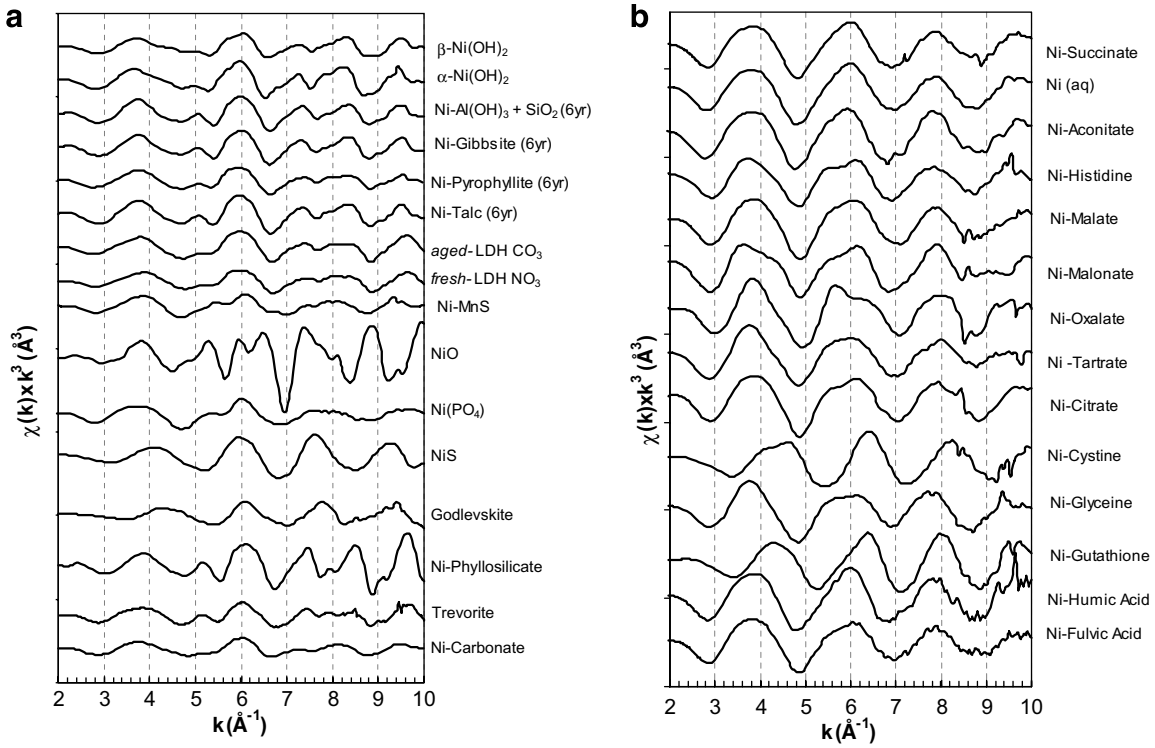

Fig. 5. Ni–K k^3 weighted χ-spectra of selected (a) mineral and (b) organic reference phases used in principal component analysis and linear least squares fitting.

soils of this study and for predicting their mobility. The 6 yr Ni–SiO_2 standard was best fit with ~6 Ni atoms at 3.10 Å in the octahedral layer, similar to that of β-$Ni(OH)_2$ indicating that the transformation to a Ni–phyllosilicate predicted by Scheckel and Sparks (2000) does not, or has not had enough time to form.

There is increasing evidence that mixed metal (e.g., Ni, Zn) layered double hydroxides (M^{n+}-Al LDH) form in field soils (Roberts et al., 1999; Manceau et al., 2000; Nachtegaal et al., 2005). As such several Ni–Al LDH samples and their precursors were included in the database (Ford et al., 1999). Two lab generated LDH precipitates were used; one with NO_3, and another with CO_3 occupying the interlayer space, and each with a Ni to Al ratio of ~2:1 (Peltier et al., 2006). Furthermore, the CO_3 interlayered LDH was aged at 65 °C for two weeks to produce a more ordered phase as would be expected with longer aging times in the natural environment. The result of the aging process is reflected in the higher second shell Al content and the slightly lower residual error (11.79 (fresh) to 8.37 (aged)) of the fit and the $\Delta\sigma^2$ values for the second shell aluminum (0.008 $Å^2$ (fresh) to 0.005 $Å^2$ (aged)) for the aged sample compared to the freshly precipitated LDH. In addition, both the alpha- and beta- type hydroxides were included with α-$Ni(OH)_2$ having a characteristically shorter Ni–Ni distance (3.10 Å) compared to the beta form (3.12 Å).

Ni–humic and Ni–fulvic acid sorption samples, as well as isolated organic and amino acid sorption standards were included in the dataset to represent the diversity of functional groups most likely present in the highly organic Quarry muck soils or as possible microbial or plant root exudates within the rhizosphere. The $k^3\chi(k)$-spectra of the organic and amino acid standards (Fig. 5b) are similar to the hexaquo-Ni standard ($Ni(H_2O)_6 \cdot NO_3$); however, there are characteristic features between 2 and 7 $Å^{-1}$ which are indicative of the binding environment of Ni. Strathmann and Myneni (2004) used both FTIR and synchrotron X-ray spectroscopies to characterize the binding environment of Ni with several organic acids. They noted that longer chain organic acids, where the carboxylate functional groups are separated by one or more methylene groups, form weak complexes with Ni, whereas those with shorter chains or closely packed carboxyl (COOH) groups supported by adjacent alcohol (C-OH) donor groups form stronger complexes, and in some cases, chelates. We found similar results using XAFS with fits for Ni -malate, -malonate, -citrate, -oxalate and –tartrate best achieved using ~3–6 C atoms at ~2.82–2.87 Å in the second coordination shell. Aconitate is similar in structure to citrate, but lacks the alcohol group at the C_3 carbon (adjacent to the carboxylic acid group) which may have reduced its ability to form chelates with Ni and likely accounted for our inability to confidently fit a carbon second shell. The amino acid histidine was fit with ~6 N/O atoms at 2.09 Å in the first shell and ~6 C atoms at 2.91 Å in the second shell which is indicative of inner-sphere complexation. The fit results were verified using ATR-FTIR (data not shown). Ni complexes with the plant/microbial antioxidant glutathione and its components (e.g., cysteine, glycine) were also included.

Table 2
Best-fit EXAFS parameters for reference mineral and sorption/precipitate samples used in principal component analysis

	Atom	First shell			Atom	Second shell			ΔE_0 (eV)	χ^2_{res}(%)
		CN	R (Å)[a]	$\Delta\sigma^2$ (Å^2)		CN	R (Å)[a]	$\Delta\sigma^2$ (Å^2)		
Minerals										
Bunsenite (NiO)	O	6.01	2.07	0.006	Ni	12.80	2.95	0.006	−4.16	3.89
Trevorite [$(Ni, Cu)Fe_2^{3+}O_4$]	O	5.07	2.06	0.004	Ni	4.79	3.07	0.007	−2.48	2.54
					Fe	3.31	2.93	0.013		
Heazlewoodite [Ni_3S_2]	S	3.96	2.25	0.007	—				−7.95	2.00
Godlevskite [$(Ni_{8.7},Fe_{0.3})_9S_8$]	S	3.25	2.32	0.003	Ni	3.27	2.52	0.03	8.69	2.74
Millerite (NiS)	S	4.45	2.33	0.008	—				3.17	2.09
Gaspeite (Ni,Mg,Fe)CO_3	O	4.83	2.07	0.005	C	2.60	2.93	0.002	2.5	13.59
Arupite ($Ni_3(PO_4)_2$)	O	6.60	2.05	0.006	—	—	—	—	−5.88	1.46
$NiCO_3$	O	5.28	2.05	0.007	Ni	3.12	3.11	0.009	−2.43	6.08
Co-precipitates										
α-$Ni(OH)_2$	O	5.60	2.04	0.005	Ni	6.15	3.10	0.006	−3.62	3.75
β-$Ni(OH)_2$	O	6.50	2.06	0.004	Ni	6.00	3.12	0.003	0.02	3.13
Ni–Al LDH (CO_3)	O	6.00	2.06	0.005	Ni	4.28	3.07	0.006	−4.72	11.00
					Al	0.50	3.07	0.008		
Aged Ni–Al LDH (CO_3)	O	5.34	2.06	0.05	Ni	2.90	3.06	0.007	−3.7	8.37
					Al	2.00	3.06	0.005		
Fresh Ni–Al LDH (NO_3)	O	5.80	2.05	0.0043	Ni	3.80	3.06	0.005	−2.64	11.79
					Al	1.60	3.06	0.005		
Ni–$Al(OH)_3$ + SiO_2 (6 yr) (i.e., Gibbsite + Quartz)	O	7.50	2.06	0.008	Ni	3.60	3.08	0.005	−2.28	1.6
					Si	7.60	3.30	0.008		
Ni Phylosilicate ($((Ni_3Si_4O_{10})OH)_2$)	O	5.60	2.06	0.003	Ni	3.65	3.06	0.001	−2.33	1.56
					Si	6.70	3.27	0.001		
Sorption samples										
Ni (aq)	O	6.70	2.05	0.006	—	—	—	—	−4.31	1.47
Ni–humic acid	O	6.60	2.06	0.003	C	1.80	2.85	0.010	−2.93	2.13
Ni–fulvic acid	O	6.60	2.04	0.007	C	2.10	2.87	0.006	2.96	5.3
Ni–gibbsite (6 yr)	O	6.00	2.04	0.006	Ni	5.30	3.08	0.009	2.5	
					Al	0.40	3.08	0.009		
Ni–SiO_2 (6 yr)	O	6.60	2.06	0.007	Ni	6.80	3.10	0.007	−1.16	7.46
Ni–talc (6 yr)	O	6.00	2.06	0.006	NI	5.70	3.09	0.008	−2.49	3.9
					Si	5.60	3.26	0.01		
Ni–pyrophyllite (6 yr)	O	7.80	2.05	0.008	Ni	6.44	3.08	0.009	−5.83	4.89
					Si	4.79	3.16	0.014		
Aqueous organic										
Ni–succinate	O	6.00	2.05	0.007		—	—	—	−0.12	2.23
Ni–aconitate	O	6.50	2.05	0.006	C	—	—	—	−0.4	9.97

(*continued on next page*)

Table 2 (*continued*)

	Atom	First shell			Atom	Second shell			ΔE_0 (eV)	χ^2_{res} (%)
		CN	R (Å)[a]	$\Delta\sigma^2$ (Å^2)		CN	R (Å)[a]	$\Delta\sigma^2$ (Å^2)		
Ni–histidine	N/O	6.40	2.09	0.005	C	5.50	2.92	0.012	−2.23	5.44
Ni–malate	O	6.00	2.05	0.002	C	3.50	2.82	0.003	1.96	6.48
Ni–malonate	O	5.90	2.03	0.004	C	3.01	2.87	0.007	−1.4	7.63
Ni–citrate	O	6.00	2.03	0.004	C	4.30	2.83	0.006	−3.52	6.76
Ni–oxalate	O	6.00	2.05	0.004	C	4.25	2.84	0.000	−1.07	6.12
Ni–tartrate	O	6.00	2.05	0.004	C	5.50	2.82	0.007	0.61	7.30
Ni–glutathione	S	2.00	2.21	0.005	C	1.67	2.91	0.001	8.4	8.34
	N	4.00	2.19	0.002	—	—	—	—		
Ni–cystine	S	4.59	2.15	0.007	C	5.43	2.93	0.007	−6.38	7.21
Ni–glycine	N	7.00	2.09	0.007	C	4.23	2.88	0.006	3.54	5.4

CN, coordination number (±20%) (Scheidegger et al., 1997).
R, inter-atomic distance (±0.02 Å for first shell and ±0.05 Å for the second and third shell (Scheidegger et al., 1997)).
σ^2(Å^2) = Debye Waller factor.
ΔE_0 = Energy shift.
(6 yr) = indicates sorption/co-precipitate samples that have been incubated for ~6 yrs at constant temperature.
[a] Bond distances derived from single shell fitting and thus represent the average radial distance.

3.5. μ-SXRF and μ-XAFS

The first step in a μ-XAFS experiment is to obtain X-ray fluorescent maps over several regions within each sample from which elemental distributions and correlations can be ascertained followed by the collection of μ-XAFS spectra at points of interest within the maps to identify the metal species. Fluorescence maps were collected over several regions within the Welland loam and Quarry muck limed and unlimed soils. Fig. 6a, for example, is a map from the un-limed Welland loam soils, in which the fluorescence signals for Ni, Fe and Mn were assigned the colors red, green and blue, respectively. Fig. 7a–d, Fig. 8a, and Fig. 9a,b are examples of maps collected from the limed loam, un-limed and limed muck soils, respectively. The color coded fluorescence signals are then superimposed with the resulting mixing of colors representative of metal associations. The color correlation triangle in the upper left corner of the μ-SXRF map is a key to interpreting the mixing of colors in the map. For example, the equal mixing of nickel (red), iron (green) and manganese (blue) fluorescence signals would appear as a white point on the map, while the equal mixing of iron (green) and manganese (blue) would result in cyan. Following this convention, the Ni, Fe and Mn distributions in the Welland loam unlimed (Fig. 6a) and limed (Fig. 7a-d) soils, as well as the unlimed and limed (Fig. 8a and Fig. 9a-b) Muck soils were visualized. Fluorescence yield from Ca, Cr, Ti, Cu, Zn and As were simultaneously collected and analyzed for their association with Ni, but no clear pattern was observed. The lack of Ni-metal associations was confirmed by cross correlating the fluorescence yield (which is proportional to the concentration) on a pixel by pixel basis for each element in the map (data not shown). Therefore, we show here the maps of Ni with Fe and Mn because they are ubiquitous in soils and provide, with reasonable detail, the structure of the soil aggregates.

As was seen in the SEM micrographs (Figs. 3 and 4), there are discrete approximately spherical Ni particles throughout the fluorescent maps of each soil (e.g., white arrow Fig. 6a). The EMPA and μ-XAFS analyses identified these particles as NiO. The stirred-flow studies showed that these particles are, for the most part, insoluble, persisting throughout the entire dissolution experiment. While the NiO particles are present in the soils and appear to dominate the EMPA and μ-SXRF maps, the removal of some Ni during the stirred-flow dissolution experiments indicate that Ni phases other than the insoluble NiO may exist. Therefore, μ-XAFS was used to probe around the obvious NiO points of interest in order to characterize the less obvious, put potentially more significant (in terms of bioavailability and reactivity) Ni species. To highlight the diffuse Ni distribution, the fluorescence yield (i.e., gamma) for Ni was increased in all of the μ-SXRF maps. By doing so the diffuse regions of Ni appear in the loam soils as red "clouds" in/on/around selected soil aggregates. In the Quarry muck soils (Figs. 8 and 9), Ni is more homogeneously distributed throughout the soil aggregates. Examples of diffuse regions of Ni can be seen in the top center of the μ-SXRF map for the un-limed Welland loam soil (Fig. 6a), or in the μ-SXRF maps for the limed Quarry

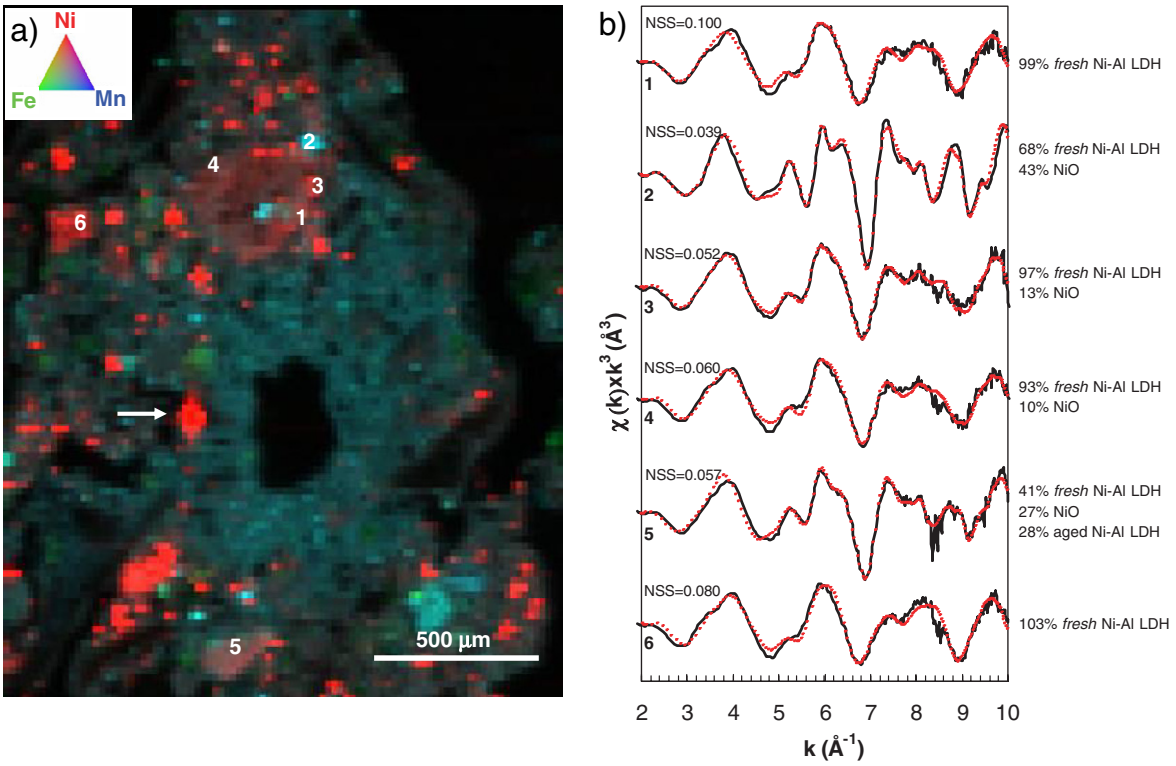

Fig. 6. (a) µ-SXRF tricolor map of the Welland loam unlimed soil and (b) µ-XAFS spectra from selected points within the map (numbers 1–6). Solid lines represent the k^3 weighted χ-spectra and the dotted lines the best fits obtained using a linear least squares fitting approach.

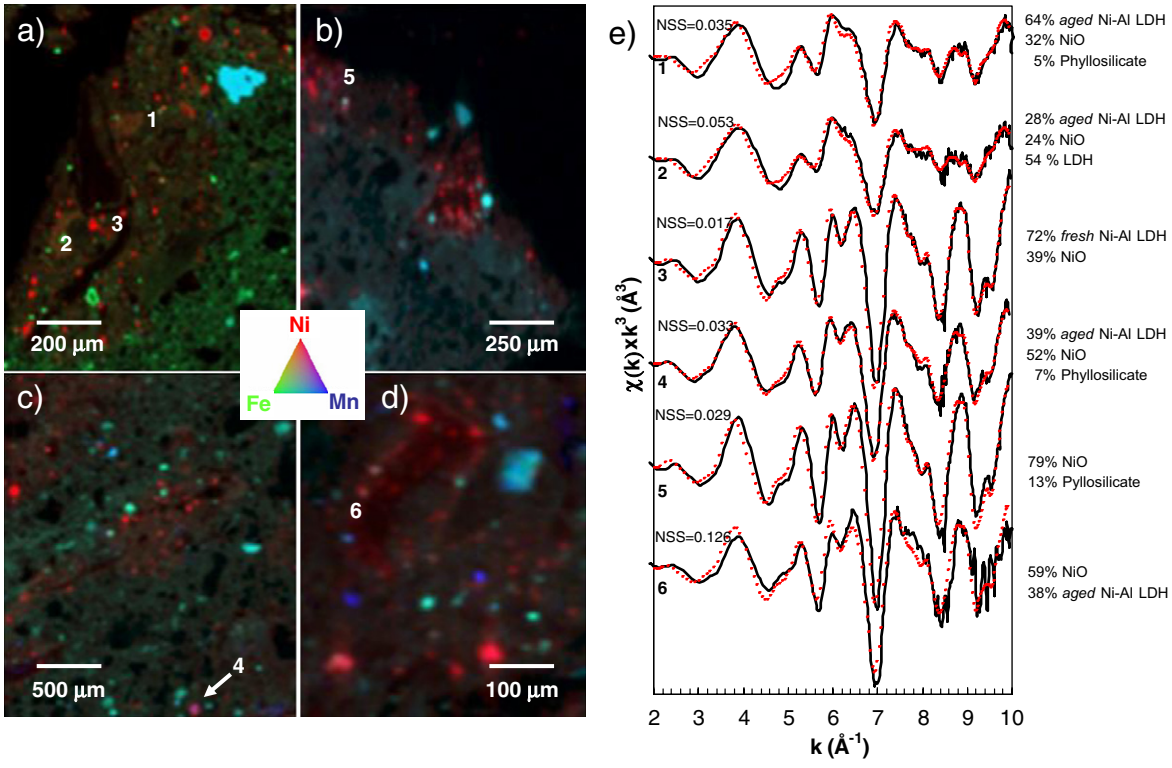

Fig. 7. (a–d) µ-SXRF tricolor map of the Welland loam limed soil and (e) µ-XAFS spectra from selected points within the maps (numbers 1–6). Solid lines represent the k^3 weighted χ-spectra and the dotted lines the best fits obtained using a linear least squares fitting approach.

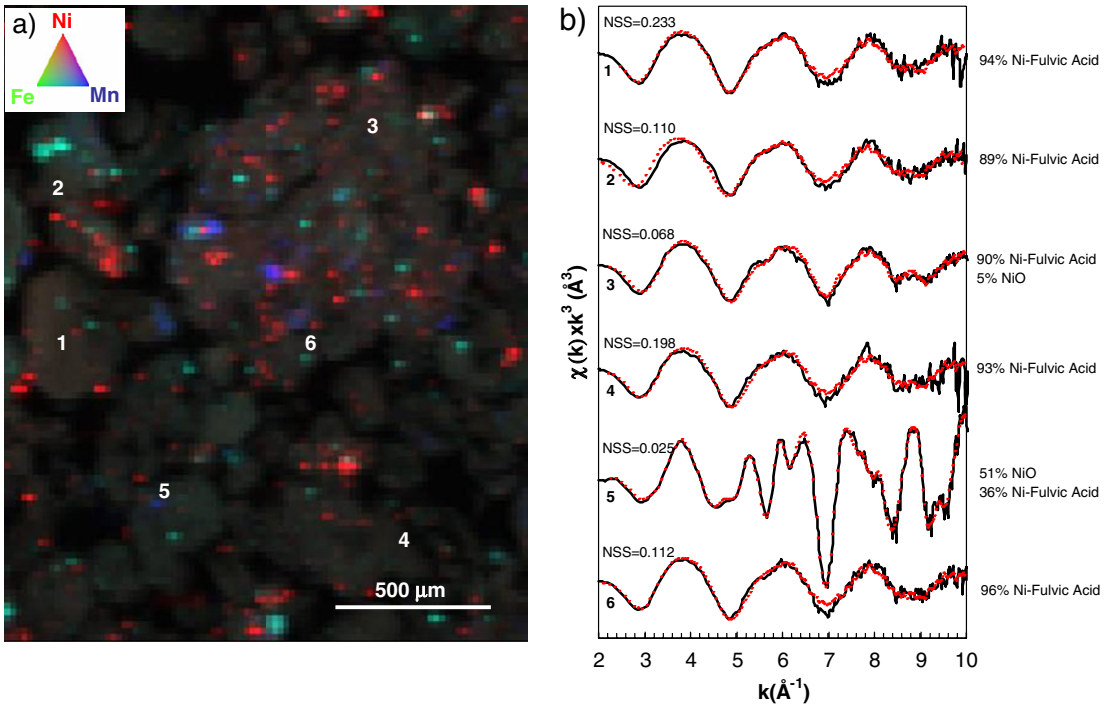

Fig. 8. (a) μ-SXRF tricolor map of the Quarry muck unlimed soil and (b) μ-XAFS spectra from selected points within the maps (numbers 1–6). Solid lines represent the k^3 weighted χ-spectra and the dotted line the best fits obtained using a linear least squares fitting approach.

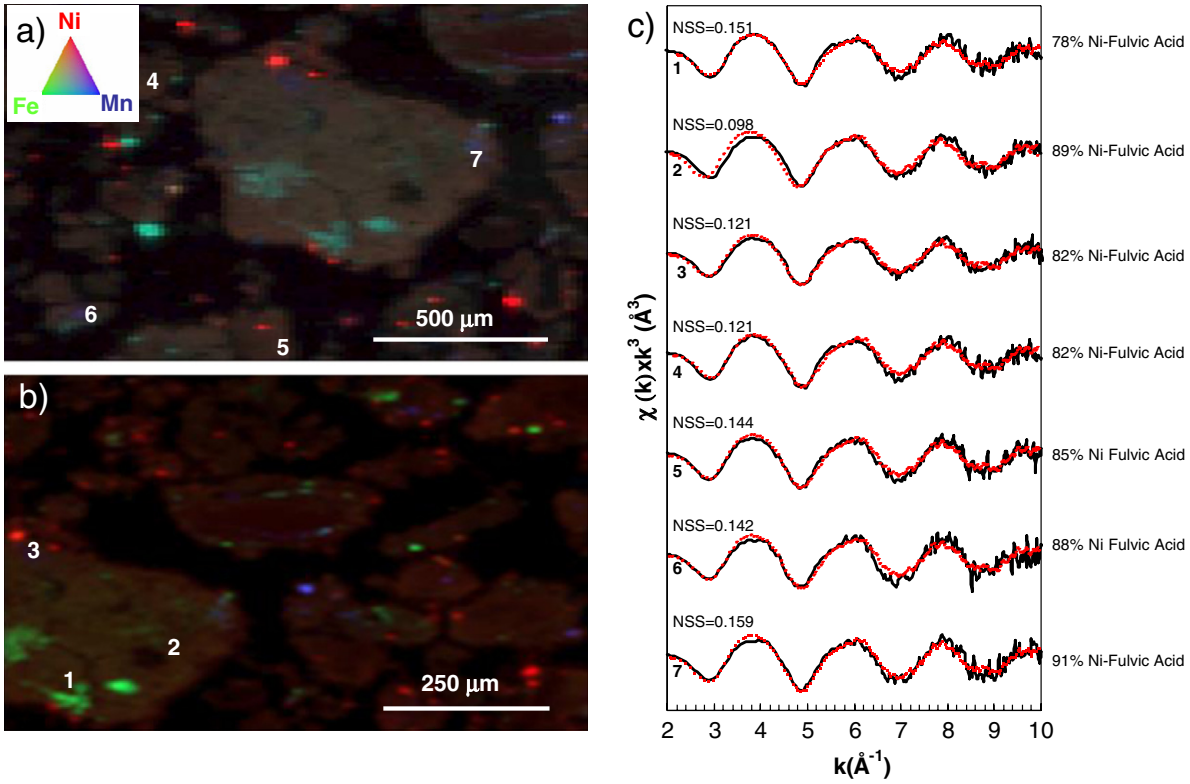

Fig. 9. (a–b) μ-SXRF tricolor map of the Quarry muck limed soil and (c) μ-XAFS spectra from selected points within the maps (numbers 1–7). Solid lines represent the k^3 weighted χ-spectra and the dotted line the best fits obtained using a linear least squares fitting approach.

muck soils (Fig. 9a and b). To obtain specific chemical and structural information about the binding environment of Ni in these areas, multiple μ-XAFS spectra were collected throughout each of the maps. Locations where μ-XAFS data were collected are indicated by numbers on the μ-SXRF maps which correspond to the adjacent $k^3\chi(k)$-spectra. The data presented here represent only a subset of the total spectra taken for each of the soils and treatments, but represent all of the Ni species identified. In all, 20 spectra were collected from the Quarry muck soils (7 limed + 13 unlimed) and 30 spectra from the Welland loam soils (11 limed + 19 unlimed). Included in these datasets were spectra from isolated silt and clay fractions from both unlimed soils as well as bulk XAFS spectra for both limed and unlimed soil types. Principal component analysis was performed on the combined (limed + un-limed) datasets for each of the soil types. PCA indicates the datasets for both the Quarry muck and Welland loam soils are best represented by three unique spectral components. To determine the most likely species represented by the principal components, target transform (TT) analysis was performed. The resulting SPOIL values for both soils can be seen in Table 3. The standard phases that received the lowest SPOIL values (from lowest to highest) in the Welland loam soils are: *fresh* NO_3 interlayered Ni–Al LDH (1.93), NiO (2.36), Ni–phyllosilicate (2.86) and an *aged* CO_3 interlayered Ni–Al LDH (3.00). For the Quarry muck soils the standard phases that received the lowest SPOIL values were NiO (2.23), Ni–fulvic acid (2.34), Ni–malate (2.53) and Ni–citrate (3.10).

Linear least squares fits were performed to determine the proportion of each of the identified standard species in the μ-EXAFS scans. The solid lines in Figs. 6b, 7e, 8b and 9c are the raw $k^3\chi(k)$-spectra and the red dotted lines the best fits using a combination of the identified reference spectra. The proportion of each of the standard phases used is located to the right of each $k^3\chi(k)$-spectra. The normalized sum square value (NSS) on the left of each spectrum is a "goodness-of-fit" parameter with lower values representing a better fit (i.e., a value of 0 = a perfect fit). The NSS values ranged from 0.017 to 0.385 (average ≈ 0.161) and 0.025 to 0.233 (average ≈ 0.116) for the Welland loam and Quarry muck soils, respectively, indicating that the 3 components used in the LLSF adequately describe the speciation in the soils.

The results of the LLSF for POI 1–6 in the μ-SXRF map for the unlimed Welland loam soil are shown in Fig. 6b. POI 1–4 and 6 were fit with all or a combination of the *fresh* NO_3 interlayerd Ni–Al LDH, and NiO standards. The best fit for point 1 was achieved using only the *fresh* Ni–Al LDH, however, it was found that the fit could be significantly improved by including reference spectra that were not identified by PCA (possibly because of a constant background or low concentration) in the LLSF. Doing so, we found that Ni–fulvic acid significantly improved the fit, resulting in a change in NSS from 0.100 to 0.056. The complexation of Ni with organic constituents in these soils is probable considering these soils contain ~9% OM. Furthermore, we saw evidence for the Ni–OM interactions in the SEM–EDX micrographs (Fig. 3), where Ni and Cu were well correlated in an organic coating around a quartz aggregate. The best fit for point 5 included the *aged* Ni–Al LDH standard which we identified as a well ordered LDH compared to the freshly precipitated variety and thus indicating a more ordered precipitate phase has formed at this location. Notably, in the μ-SXRF map, the color mixing at point 5 appears slightly more uniform than points 1–4 and 6, and the particle more angular, which may indicate that the precipitate at this point is present as a coating on a clay particle. Similar POI were seen in the limed loam samples (Fig. 7), specifically points 1, 4 and 5, which in addition to the *aged* Ni–Al LDH species, also included Ni–phyllosilicate. The $\chi(k)k^3$-spectra collected from the limed loam soils have more structure compared to the unlimed loam soils, with a "doublet" peak between 6.5 $Å^{-1}$

Table 3
Target transform SPOIL values using three components for the Quarry muck and Welland loam soils

	SPOIL value*	
	Quarry Muck	Welland loam
Minerals		
Bunsenite (NiO)	**2.23**	**2.36**
Trevorite [$(Ni,Cu)Fe_2^{3+}O_4$]	10.88	3.85
Heazlewoodite [Ni_3S_2]	8.96	7.59
Godlevskite [$(Ni_{8.7},Fe_{0.3})_9S_8$]	14.53	7.34
Millerite (β-NiS)	12.78	6.81
Gaspeite (Ni,Mg,Fe)CO_3	10.11	4.46
Arupite ($Ni_3(PO_4)_2$)	6.59	5.43
$NiCO_3$	6.21	3.70
Co-precipitates		
α-$Ni(OH)_2$	10.55	5.73
β-$Ni(OH)_2$	8.73	5.19
Ni–Al LDH (CO_3)	8.79	3.18
Aged Ni–Al LDH (CO_3)	8.19	**3.00**
Fresh Ni–Al LDH (NO_3)	7.37	**1.93**
Ni–$Al(OH)_3$ + SiO_2 (6 yr) (i.e., Gibbsite + Quartz)	13.10	6.34
Ni phylosilicate $(((Ni_3Si_4O_{10})OH)_2)$	16.52	**2.86**
Sorption samples		
Ni (aq)	3.44	3.31
Ni–humic acid	5.00	4.44
Ni–fulvic acid	**2.34**	3.73
Ni–gibbsite (6 yr)	13.25	6.17
Ni–SiO_2 (6 yr)	13.01	5.69
Ni–talc (6 yr)	10.78	5.42
Ni–pyrophyllite (6 yr)	8.53	5.11
Aqueous organic		
Ni–aconitate	3.47	3.69
Ni–histidine	3.71	4.34
Ni–malate	**2.53**	3.70
Ni–malonate	3.58	3.79
Ni–citrate	**3.10**	4.03
Ni–oxalate	5.17	4.26
Ni–tartrate	3.82	3.89
Ni–glutathione	16.25	13.42
Ni–cystine	14.25	23.49
Ni–glycine	5.56	4.65

In bold are the references used in the linear least squares fits.
* SPOIL values <1.5 indicate an excellent fit, 1.5–3 good, 3–4.5 fair, 4.5–6 poor, and values >6 are unacceptable.

and the deep trough at 7 $Å^{-1}$ which are characteristics of strong backscattering from highly ordered phases such as NiO.

To summarize, the average Ni distribution using μ-XAFS and PCA-LLSF in all of the spots analyzed from the diffuse regions in both the limed and un-limed Welland loam soils combined is: *fresh* Ni–Al LDH (NO_3) (56%) > aged Ni Al LDH (CO_3) (21%) ≈ NiO (20%) > Ni–phyllosilicate (1%). The average Ni distribution in the diffuse regions of the unlimed soils only is: *fresh* Ni Al LDH (NO_3) (66%) > aged Ni–Al LDH (CO_3) (15%) ≈ NiO (12%). The average distribution in the limed soils only is: *fresh* Ni–Al LDH (NO_3) (39%) ≈ NiO (33%) > *aged* Ni–Al LDH (15%) > Ni phyllosilicate (2%). Clearly, the Ni–Al LDH precipitates make up a large portion of the Ni speciation within the diffuse areas in both the limed and un-limed Welland loam soils. To determine the contribution of these secondary Ni phases to the overall Ni speciation within the Welland loam limed and unlimed soils, LLSF were done using the bulk XAFS spectra, and the species identified in PCA (Fig. 10a). The two bulk XAFS spectra look very similar, each showing dampening and slight splitting at ~8 $Å^{-1}$, which is typically interpreted as a contribution from multiple scattering events with Al in the Ni–Al LDH. The spectra are fit well using two components, NiO and the Ni–Al LDH. Notably, unlike in the LLSF for the μ-XAFS spectra, the *fresh* and *aged* Ni–Al LDH were interchangeable in the fit; the subtleties of each most likely masked by the overlapping contributions in the bulk spectra. Additionally, inclusion of a Ni phyllosilicate phase did not improve the fit, further highlighting the effectiveness of μ-XAFS techniques at detecting minor components.

The results for the LLSF of the POI in the μ-SXRF map for the unlimed Quarry muck soil can be seen in Fig. 8b. With the exception of point 5, the spectra are strongly sinusoidal out to ~10 $Å^{-1}$ with a slight split at ~6 $Å^{-1}$. POI 1, 2, 4 and 6 were best fit using Ni–fulvic acid only, while points 3 and 5 contained significant amounts of NiO. In the limed soils (Fig. 9c), only the Ni–fulvic acid standard produced the best fits. PCA indicated that there were 3 components necessary to reproduce the dataset, yet only NiO and Ni–FA provided best fits in our analysis. The most likely explanation is that fulvic acid is comprised of a mixture of functional groups (the most prominent being –COOH) each capable of sequestering Ni and other metals in a unique configuration. This FA "mixture" does a reasonable job of fitting the average coordination environment of Ni in the sites analyzed in our samples. Comparing the two treatments, we were better able to fit the sum (i.e., % total contribution of the standard to the unknown) of the spectra for the unlimed muck soils (92%) compared to the limed soils (85%). Several factors, including pH, can have a pronounced impact on the morphology of soil humic and fulvic acids which may have lead to a more disordered

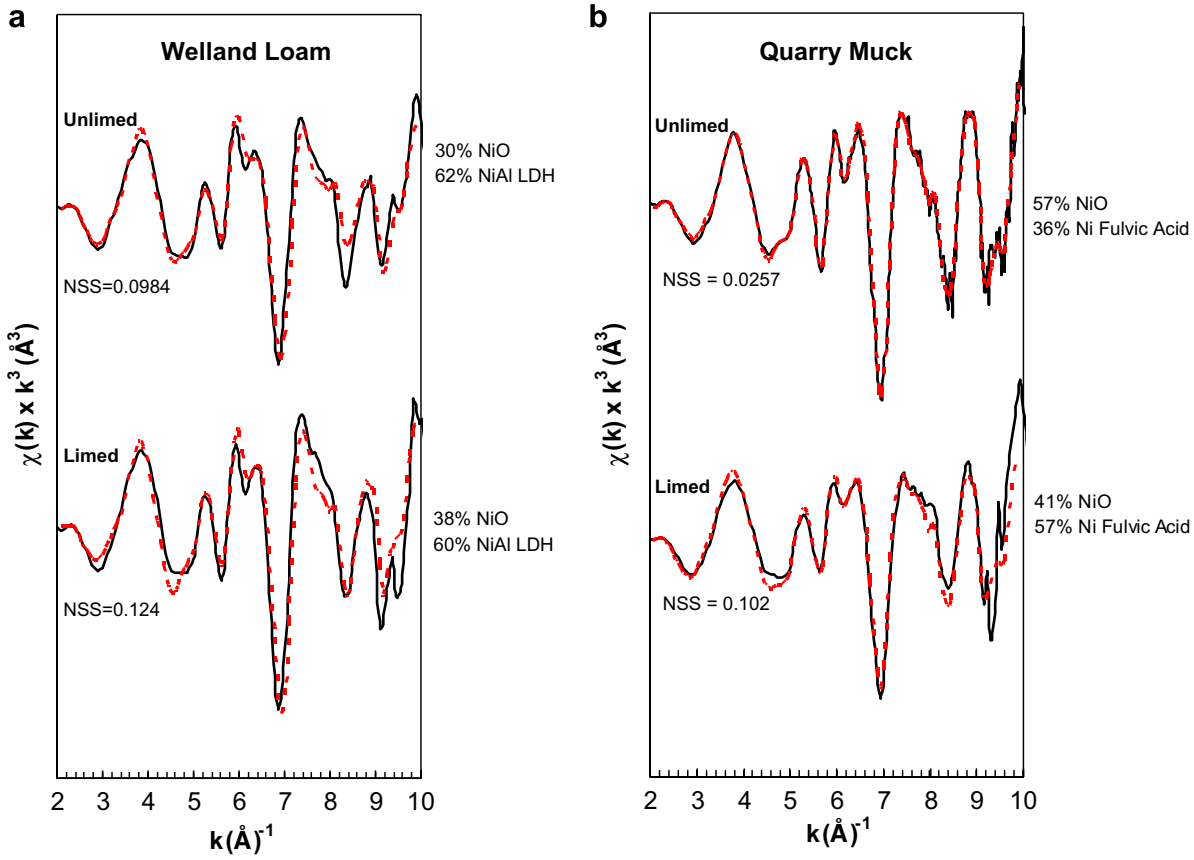

Fig. 10. Best fits of the bulk EXAFS spectra from the (a) unlimed and limed Welland loam and (b) Quarry muck soils. Solid lines represent the k^3 weighted χ-spectra and the dotted line the best fits obtained using a linear least squares fitting approach.

binding environment (Myneni et al., 1999) and thus inferior fits for the unlimed soils. Conversely, the functional groups partaking in the sequestration of Ni and/or the configuration of Ni binding changes with increased pH; a configuration which may not be well represented in our present standard dataset.

Fits of the bulk, limed and unlimed Quarry muck soils can be seen in Fig. 10b. Much like the Welland soils, the limed and unlimed Quarry muck spectra look similar, closely resembling the spectra of NiO. The fit for the unlimed soil was very good (NSS = 0.0257) compared to the limed soil (NSS = 0.102). The fit had trouble reproducing the features between 4 and 5$Å^{-1}$ and the trough at ~8.4 $Å^{-1}$. These features are slightly dampened compared to those in the unlimed soil, as well as the NiO standard; likely due to the increased amount of organically bound Ni.

3.6. Summary of Ni Speciation, mobility and bioavailability

The objectives of this research were to determine the effect of soil type and treatment on the speciation of Ni in Welland loam and Quarry muck soils surrounding an historic nickel refinery in Port Colborne, Ontario, Canada. Using a combination of methods, we determined that NiO is the common Ni species in both the Welland loam and Quarry muck soils. Electron microscopy and μ-SXRF showed that the NiO particles have an approximately spherical morphology, are ~10–50 μm in diameter and are associated with no other metals.

According to the materials safety data sheets for NiO, it is considered soluble in acids, potassium cyanide and ammonium hydroxide but insoluble in both cold and hot water and caustic solutions. However, nickel solubility is highly dependent on the type of NiO which can vary with the process used to produce it as well as the mineral source from which it was derived. The most common forms of NiO are the more crystalline black NiO, which has higher oxygen content than green nickel oxide; the other common form. A wide range in NiO solubility has been shown by several researchers (Takahashi et al., 1992; Yamada et al., 1993; Takahashi et al., 1999), in which they demonstrated that the green form of NiO was less soluble than the black form. The dissolution of Ni from the black forms was attributed to Ni carbonate impurities (~1%) which quickly dissolved upon reaction with water. Our XAFS standard analyses are based on the *green*-NiO form, however it is unlikely that distinguishable differences exist in the XAFS spectra from the two types. Attempts were not made here to distinguish between the types of NiO present in the Port Colborne soils. Regardless, it is very likely that any impurities that may have existed within the NiO particles have since dissolved over the ~70 yrs since their initial deposition. The NiO that remains is very resistant to weathering as indicated by the stirred-flow studies during which only ~2% of the total Ni was released from the un-limed soils. These findings indicate that the NiO is very stable and will likely remain in the soils for many years.

The μ-XAFS analysis of the Quarry muck soils revealed that Ni– fulvic acid (FA) dominated the speciation within the diffuse regions of the Quarry muck soils. Interestingly, many of the organic acid (OA) standards used in the PCA had SPOIL values that were several orders of magnitude better than the inorganic standards (Table 3). The reason for this is likely due to the fulvic acid standard being comprised of a mixture of functional groups with the most prominent being carboxylate (–COOH), which can bind Ni in a variety of configurations. When we exclude the FA standard from the LLSF and included the third and fourth most likely components, Ni–malate and Ni–citrate, we found that almost identical fits (evaluated by comparing the NSS value of the fit with and without FA) were obtained for most sample spectra (data not shown). While citric and malic acids are found in the rhizosphere as exudates from plant roots or microbes, it is unlikely that these are the exact components being fit in the PCA-LLSF analysis. In a study looking for an analog for dissolved organic matter in natural waters, MacRae et al. (1999) found that the three organic acids, dipicolinic, oxalic and malonic, mimicked the copper binding properties of DOM in stream waters. Similarly, in our soils, it is likely that citric and malic acid serve as proxies for the different coordination environments encountered by Ni in the Muck soils. Interestingly, in the unlimed (pH 5.8) soils, a larger fraction of the Ni complexation could be attributed to Ni–malate, while in the limed (pH 6.5) soils we saw a higher proportion of the Ni complexed with citrate. Helling et al. (1964) and Yuan et al. (1967) have clearly shown that the CEC of a soil significantly increases with pH as acidic groups (namely COOH) are ionized. Even the small change in pH observed in our soils could result in orders of magnitude greater CEC and therefore a noticeable change in the coordination environment of Ni. Therefore, the presence of more stable Ni–OA complexes (i.e., Ni–citrate) in the limed soils gives spectroscopic evidence for the stronger binding of Ni in these soils and explains the reduction in Ni desorption in the stirred-flow studies as well as the reduction in plant available Ni in other studies on these soils (Frank et al., 1982; Kukier and Chaney, 2000; Kukier and Chaney, 2001).

The μ-XAFS, μ-SXRF investigation of the subsidiary phases in the loam soils found that secondary precipitates of Ni and Al were the prevalent species in both the unlimed (pH 7) and limed (pH 7.5) soils. Several studies have demonstrated that Zn LDH and phyllosilicate precursor phases can form in soil surrounding Zn smelters (Manceau et al., 2000; Roberts et al., 2002; Nachtegaal et al., 2005). Additionally, Roberts et al. (1999) using bulk XAFS found that Ni–Al LDH precipitates formed in ~24 h in a lab contaminated whole soil at pH 7.5. The pH of the loam soils in this study was high enough, even in the unlimed soil, to facilitate the formation of LDH phases. Further supporting these findings, Peltier et al. (2006) compared the enthalpies of formation of various Ni precipitates and found that the formation of Ni–Al LDH phases are thermodynamically favored over nickel hydroxide precipitates in soils containing soluble Al, especially at pH values $\geqslant$6.5. Substitution of Si for the interlayer anion of the Ni–Al LDH phases was also determined to be thermodynamically favored resulting in the formation of more stable Ni phyllosilicate phases. Therefore, the pH of the Welland loam soils (7.0–7.5) and

the presence of Al bearing minerals (e.g., kaolinite) may have facilitated the formation of Ni–Al LDH phases and, with liming (and higher Si solubility), the formation of Ni phyllosilicates. The formation of these more stable phases likely accounts for the reduction in Ni loss from the limed loam soil observed in the stirred-flow experiments and the reduction in Ni toxicity symptoms in the crops tested in previous studies on these soils.

4. CONCLUSIONS

This work gives the first evidence of Ni–Al LDH phases forming in situ in field soils contaminated via anthropogenic processes. Like other accounts examining Zn speciation in smelter soils, we found that LDH phases can account for a significant portion of the soil metal speciation. The results from this study support a scenario in which any soluble Ni species aerially deposited from the refinery into the Quarry muck and Welland loam soils, as well as, Ni atoms released form the persistent NiO particles, have since or continue to be incorporated into secondary phases (e.g., precipitates or organic complexes). The persistence of the NiO particles will complicate attempts to reduce Ni concentrations below the Canadian MOE requirements of 200 mg/kg using phytoremediation alone, because it is unlikely that the plant is capable of accessing Ni from NiO. Interestingly, increased accumulation by *A. murale* with increasing pH indicates that the plant may be capable of removing Ni from either the LDH phases or the Ni fraction strongly complexed to organic matter in the loam or muck soils, respectively; phases typically considered unavailable to plants. It has yet to be shown how bioavailable these phases are to *A. murale*, if one phase is more "available" than another or the mechanisms used by *A. murale* to more efficiently remove Ni at higher pH; all topics of ongoing research.

ACKNOWLEDGMENTS

The authors would like to thank Kirk Scheckel, Andreas Scheinost, Ted Peltier, Maarten Nachtegaal and Timothy Strathman for supplying XAFS spectra for selected references. We would like to thank Matthew Marcus for assistance with μ-XAFS data collection at the Advanced Light Source beamline 10.3.2 and the staff of beamline X11A at the National Synchrotron Light Source (NSLS) for their assistance in the collection of the EXAFS standards spectra. The Advanced Light Source is supported by the Director, Office of Science, Office of Basic Energy Sciences, of the U.S. Department of Energy under Contract No. DE-AC02-05CH11231. Use of the National Synchrotron Light Source, Brookhaven National Laboratory, was supported by the U.S. Department of Energy, Office of Science, Office of Basic Energy Sciences, under Contract No. DE-AC02-98CH10886. We would also like to thank Ken Livi of the Department of Earth and Planetary Sciences at Johns Hopkins University for help with EMPA data collection, analysis and interpretation. The authors would also like to thank all reviewers for their constructive comments and advice.

REFERENCES

Bacon W. G., Dalvi A. D., Rochon B. A., and Selby M. (2002) Nickel outlook—2000 to 2010. *Cim Bull.* **95**, 47–52.

Bisessar S. (1989) Effects of lime on nickel uptake and toxicity in celery grown on muck soil contaminated by a nickel refinery. *Sci. Total Environ.* **84**, 83–90.

Burkin A. R. (ed.) (1987) *Extractive Metallurgy of Nickel*. Wiley, Chichester, New York.

Fleet M. E. (1977) The crystal structure of heazlewoodite, and metallic bonds in sulfide minerals. *Am. Mineral.* **62**, 341–345.

Ford R. G., Scheinost A. C., Scheckel K. G., and Sparks D. L. (1999) The link between clay mineral weathering and the stabilization of Ni surface precipitates. *Environ. Sci. Technol.* **33**, 3140–3144.

Frank R., Stonefield K. I., Suda P., and Potter J. W. (1982) Impact of nickel contamination on the production of vegetables on an organic soil. Ontario, Canada, 1980–1981. *Sci. Total Environ.* **26**, 41–65.

Génin P., Delahaye-Vidal A., Portemer F., Tekaia-Elhsissen K., and Figlarz M. (1991) Preparation and characterization of a-type nickel hydroxides obtained by chemical precipitation: Study of the anionic species. *Eur. J. Solid. State Inorg. Chem.* **28**, 505–518.

Grice J. D., and Ferguson R. B. (1974) Crystal structure refinement of millerite (β-NiS). *Can. Mineral.* **12**, 248–252.

Helling C. S., Chesters C., and Corey R. B. (1964) Contribution of organic matter and clay to soil cation-exchange capacity as affected by the pH of the saturating solution. *Soil Sci. Soc. Am. Proc.* **28**, 517–520.

Hoflich B. L. W., Wentzel M., Ortner H. M., Weinbruch S., Skogstad A., Hetland S., Thomassen Y., Chaschin V. P., and Nieboer E. (2000) Chemical composition of individual aerosol particles from working areas in a nickel refinery. *J. Environ. Monit.* **2**, 213–217.

Kuja A., Jones R., and McIlveen W. (2000) Phytotoxicology soil investigation: INCO-Port Colborne 1999. Phytotoxicology and Soils Standards Section. Rep. No. SDB-031-3511-2000. Standards Development Branch, Ontario, Ministry of the Environment, Queen's Printer of Ontario, Toronto, Canada.

Kukier U., and Chaney R. L. (2000) Remediating Ni-phytotoxicity of contaminated Quarry muck soil using limestone and hydrous iron oxide. *Can. J. Soil Sci.* **80**, 581–593.

Kukier U., and Chaney R. L. (2001) Amelioration of nickel phytotoxicity in muck and mineral soils. *J. Environ. Qual.* **30**, 1949–1960.

Kukier U., and Chaney R. L. (2004) In-situ remediation of nickel phytotoxicity for different plant species. *J. Plant Nutr.* **27**, 465–495.

Lavkulic L. M., and Wiens J. H. (1970) Comparison of Organic Matter Destruction by Hydrogen Peroxide and Sodium Hypochlorite and Its Effects on Selected Mineral Constituents. *Soil Sci. Soc. Am. Proc.* **34**, 755.

Li Y. M., Chaney R., Brewer E., Roseberg R., Angle J. S., Baker A., Reeves R., and Nelkin J. (2003) Development of a technology for commercial phytoextraction of nickel: economic and technical considerations. *Plant Soil* **249**, 107–115.

MacRae R. K., Maest A. S., and Meyer J. S. (1999) Selection of an organic acid analogue of dissolved organic matter for use in toxicity testing. *Can. J. Fish. Aquat. Sci.* **56**, 1484–1493.

Malinowski E. R. (1977) Determination of the number of factors and the experimental error in a data matrix. *Anal. Chim. Acta* **49**, 612–617.

Malinowski E. R. (1978) Theory of error for target factor analysis with applications to mass spectrometry and nuclear magnetic resonance spectrometry. *Anal. Chim. Acta* **103**, 354–359.

Manceau A., Lanson B., Schlegel M. L., Harge J. C., Musso M., Eybert-Berard L., Hazemann J. L., Chateigner D., and Lamble G. M. (2000) Quantitative Zn speciation in smelter-contaminated soils by EXAFS spectroscopy. *Am. J. Sci.* **300**, 289–343.

Manceau A., Marcus M. A., and Tamura N. (2002) Quantitative speciation of heavy metals in soils and sediments by synchrotron X-ray techniques. In *Applications of Synchrotron Radiation in Low-temperature Geochemistry and Environmental Sciences* vol. 49 (eds. P. A. Fenter, M. L. Rivers, N. C. Sturchio and S. R. Sutton). Mineralogical Society of America, pp. 341–428.

Marcus M. A., MacDowell A. A., Celestre R., Manceau A., Miller T., Padmore H. A., and Sublett R. E. (2004) Beamline 10.3.2 at ALS: a hard X-ray microprobe for environmental and materials sciences. *J. Synch. Rad.* **11**, 239–247.

Mehra O. P., and Jackson M. L. (1960) Iron oxide removal from soils and clays by dithionite-citrate-system buffered with sodium bicarbonate. *Clays Clay Miner.* **7**, 317–327.

Myneni S. C. B., Brown J., Martinez G. A., and Meyer-Ilse W. (1999) Imaging of humic substance macromolecular structures in water and soils. *Science* **286**, 1335–1337.

Nachtegaal M., Marcus M. A., Sonke J. E., Vangronsveld J., Livi K. J. T., van der Lelie D., and Sparks D. L. (2005) Effects of in-situ remediation on the speciation and bioavailability of zinc in a smelter contaminated soil. *Geochim. Cosmochim. Acta* **69**, 4649–4664.

Nachtegaal M., and Sparks D. L. (2003) Nickel sequestration in a kaolinite-humic acid complex. *Environ. Sci. Technol.* **37**, 529–534.

Nicolai B., Kearley G. J., Johnson M. R., Fillaux F., and Suard E. (1998) Crystal structure and low-temperature methyl-group dynamics of cobalt and nickel acetates. *J. Chem. Phys.* **109**, 9062–9074.

Nriagu J. O. (1996) A history of global metal pollution. *Science* **272**, 223–224.

O'Day P. A., Parks G. A., and Brown G. E. (1994) Molecular structure and binding sites of cobalt(II) surface complexes on kaolinite from X-ray absorption spectroscopy. *Clays Clay Miner.* **42**, 337–355.

Peltier E., Allada R. K., Navrotsky A., and Sparks D. L. (2006) Nickel solubility and precipitation in soils: a thermodynamic study. *Clays Clay Miner.* **54**, 153–163.

Raskin I., Smith R. D., and Salt D. E. (1997) Phytoremediation of metals: using plants to remove pollutants from the environment. *Curr. Opin. Biotech.* **8**, 221–226.

Ressler T. (1997) WinXAS: a new software package not only for the analysis of energy-dispersive XAS data. *J. Phys. IV* **7**, 269–270.

Roberts D. R., Scheidegger A. M., and Sparks D. L. (1999) Kinetics of mixed Ni–Al precipitate formation on a soil clay fraction. *Environ. Sci. Technol.* **33**, 3749–3754.

Roberts D. R., Scheinost A. C., and Sparks D. L. (2002) Zinc speciation in a smelter-contaminated soil profile using bulk and microspectroscopic techniques. *Environ. Sci. Technol.* **36**, 1742–1750.

Santoro A., Mighell A. D., Zocchi M., and Reimann C. W. (1969) The crystal and molecular structure of hexakis(imidazole) nickel(II) nitrate, $(C_3H_4N_2)_6Ni(NO_3)_2$. *Acta Crystallogr., Sect. B: Struct. Sci.* **B25**, 842–847.

Sarret G., Saumitou-Laprade P., Bert V., Proux O., Hazemann J. L., Traverse A. S., Marcus M. A., and Manceau A. (2002) Forms of zinc accumulated in the hyperaccumulator Arabidopsis halleri. *Plant Phys.* **130**, 1815–1826.

Scheckel K. G., Scheinost A. C., Ford R. G., and Sparks D. L. (2000) Stability of layered Ni hydroxide surface precipitates - A dissolution kinetics study. *Geochim. Cosmochim. Acta* **64**, 2727–2735.

Scheckel K. G., and Sparks D. L. (2000) Kinetics of the formation and dissolution of Ni precipitates in a gibbsite/amorphous silica mixture. *J. Colloid Interface Sci.* **229**, 222–229.

Scheckel K. G., and Sparks D. L. (2001) Dissolution kinetics of nickel surface precipitates on clay minerals and oxide surfaces. *Soil Sci. Soc. Am. J.* **65**, 685–694.

Scheidegger A. M., Lamble G. M., and Sparks D. L. (1997) The kinetics of nickel sorption on pyrophyllite as monitored by x-ray absorption fine structure (XAFS) spectroscopy. *J. Phys. IV* **7**, 773–775.

Scheidegger A. M., Strawn D. G., Lamble G. M., and Sparks D. L. (1998) The kinetics of mixed Ni–Al hydroxide formation on clay and aluminum oxide minerals: a time-resolved XAFS study. *Geochim. Cosmochim. Acta* **62**, 2233–2245.

Scheinost A. C., Ford R. G., and Sparks D. L. (1999) The role of Al in the formation of secondary Ni precipitates on pyrophyllite, gibbsite, talc, and amorphous silica: a DRS study. *Geochim. Cosmochim. Acta* **63**, 3193–3203.

Scheinost A. C., and Sparks D. L. (2000) Formation of layered single- and double-metal hydroxide precipitates at the mineral/water interface: a multiple-scattering XAFS analysis. *J. Colloid Interface Sci.* **223**, 167–178.

Stewart J. M., Lingafelter E. C., and Breazeale J. D. (1961) The crystal structue of Disaguabis(salicylaldehydato) nickel. *Acta Cryst.* **14**, 888–891.

Strathmann T. J., and Myneni S. C. B. (2004) Speciation of aqueous Ni(II)-carboxylate and Ni(II)-fulvic acid solutions: combined ATR-FTIR and XAFS analysis. *Geochim. Cosmochim. Acta* **68**, 3441–3458.

Strawn D. G., and Sparks D. L. (2000) Effects of soil organic matter on the kinetics and mechanisms of Pb(II) sorption and desorption in soil. *Soil Sci. Soc. Am. J.* **64**, 144–156.

Sumner M. E., Miller W. P. (1996) Cation exchange capacity and exchange coefficients. In *Methods Of Soil Analysis Part 3 Chemical Methods*, third ed. (ed. D. Sparks). Soil Science Society of America, Madison, WI, pp. 1201–1229.

Takahashi S., Oishi M., Takeda E., Kubota Y., Kikuchi T., and Furuya K. (1999) Physicochemical characteristics and toxicity of nickel oxide particles calcined at different temperatures. *Biol. Trace Elem. Res.* **69**, 161–174.

Takahashi S., Yamada M., Kondo T., Sato H., Furuya K., and Tanaka I. (1992) Cytotoxicity of nickel oxide particles in rat alveolar macrophages. *J. Toxicol. Sci.* **17**, 243–251.

Taylor R. M. (1984) The rapid formation of crystalline double hydroxy salts and other compounds by controlled hydrolysis. *Clay Miner.* **19**, 591–603.

Temple P. J., and Bisessar S. (1981) Uptake and toxicity of nickel and other metals in crops grown on soil contaminated by a nickel refinery. *J. Plant Nutr.* **3**, 473–482.

Trivedi P., Axe L., and Tyson T. A. (2001) XAS studies of Ni and Zn sorbed to hydrous manganese oxide. *Environ. Sci. Technol.* **35**, 4515–4521.

Voegelin A., Pfister S., Scheinost A. C., Marcus M. A., and Kretzschmar R. (2005) Changes in zinc speciation in field soil after contamination with zinc oxide. *Environ. Sci. Technol.* **39**, 6616–6623.

Wasserman S. R., Allen P. G., Shuh D. K., Bucher J. J., and Edelstein N. M. (1999) EXAFS and principal component analysis: a new shell game. *J. Synchro. Rad.* **6**, 284–286.

Weinbruch S., Van Aken P., Ebert M., Thomassen Y., Skogstad A., Chashchin V. P., and Nikonov A. (2002) The heterogeneous composition of working place aerosols in a nickel refinery: a transmission and scanning electron microscope study. *J. Environ. Monit.* **4**, 344–350.

Yamada M., Takahashi S., Sato H., Kondo T., Kikuchi T., Furuya K., and Tanaka I. (1993) Solubility of nickel oxide particles in various solutions and rat alveolar. *Biol. Trace Elem. Res.* **36**, 89–98.

Yuan T. L., Gammon Jr. N., and Leighty R. G. (1967) Relative contribution of organic and clay fractions to cation-exchange capacity of sandy soils from several groups. *Soil Sci.* **104**, 123–128.

Zabinsky S. I., Rehr J. J., Ankudinov A., Albers R. C., and Eller M. J. (1995) Multiple scattering calculations of X-ray absorption spectra. *Phys. Rev. B* **52**, 2995.

Associate editor: Chen Zhu